RSC Chemical Biology

ROYAL SOCIETY OF CHEMISTRY

PAPER

View Article Online
View Journal

Cite this: DOI: 10.1039/d6cb00112b

Native MS and ligand observed NMR uncovers subtle SLiM binding variations that mediate HSP90-Hop PPI modulation

Tara K. Davids, †[a] Daniel A. Kusza, †[a] Shannon K. Misplon,[a] Josef C. Späth,[a] Richwell Mhlanga,[b] David J. Clarke,[c] Beatriz G. de la Torre,[d] Fernando Albericio,[e] Adrienne L. Edkins,[b] Marwaan Rylands *[a] and Clinton G. L. Veale *[a]

We have previously demonstrated that a non-natural tetrazole containing peptide (**2**), which mimics the MEEVD Short Linear Motif (SLiM) found at the Heat Shock Protein 90 (HSP90) C-terminus, disrupts the transient protein–protein interaction (PPI) formed between HSP90 and the HSP70-HSP90 organizing protein (Hop) co-chaperone. However, the native MEEVD SLiM (**1**) showed negligible inhibitory activity despite similar binding affinity to the interacting Hop_{TPR2A} domain. To investigate the origin of this discrepancy, we combined native mass spectrometry (nMS) coupled to ion mobility (IM) with saturation transfer difference (STD) and water ligand observed *via* gradient spectroscopy (WLOGSY) NMR to interrogate the interaction of peptides **1** and **2** alongside a series of peptide derivatives with Hop_{TPR2A}. Collectively, these data revealed that the variation in sequence between peptides **1** and **2** imparts subtle variations in conformational stability and magnetization transfer, indicating that differences in PPI modulation arise from altered binding mode rather than binding affinity. These results not only provide a structural framework for developing peptidomimetic HSP90-Hop PPI inhibitors, but a generalized strategy for exploiting transient PPIs for drug discovery.

Received 21st March 2026,
Accepted 5th May 2026

DOI: 10.1039/d6cb00112b

rsc.li/rsc-chembio

Introduction

Transient protein–protein interactions (PPIs), play a central role as mediators of biological pathways, cell metabolism and signalling networks. Minor alterations in the interfacial interactions of PPIs, whether they occur from sequence mutation, or small molecule modulation can have considerable biological consequences,[1–3] rendering them attractive targets for addressing unmet medical needs.[4] The necessity for specific, low-affinity interactions means that PPIs are typically mediated by the interaction between a disordered short linear motif (SLiM) with a corresponding binding domain. However, the short lived and dynamic nature of these interactions mean that both the interfacial characterization and identification of PPI modulators is a significant challenge.[4,5] In addressing the structural characterization problem, the X-ray crystallography community identified that the simplified SLiM-domain interaction in isolation, is often sufficient for characterizing the primary interfacial interactions of PPIs.[6,7] The revelation that SLiM-domain interactions act as models of transient PPIs paved the way for orthogonal biophysical methodologies, often with comparatively simpler experimental set ups to be employed to elucidate additional temperature-sensitive structural details of PPI interfaces.[8,9] Two examples of these orthogonal biophysical methods are native mass spectrometry (nMS) and ligand-observed nuclear magnetic resonance (NMR), which not only possess the ability to interrogate SLiM-domain interactions, but critically, small molecule induced modulation of these PPI models.[10–13] In addition, ion mobility (IM) has emerged as a complimentary hyphenated technique for nMS. Briefly, IM experiments involve the translocation of ions, under the influence of an electric field, through a cell filled with inert gas. Under these conditions, ions can be distinguished based on their differences in charge, size and shape and is reflected in differences in drift times. In the context of nMS, this data provides insights into the

[a] Department of Chemistry, University of Cape Town, Rondebosch, Cape Town 7701, South Africa. E-mail: Marwaan.rylands@uct.ac.za, Clinton.veale@uct.ac.za
[b] The Biomedical Biotechnology Research Unit (BioBRU), Department of Biochemistry and Microbiology, Rhodes University, Makhanda, 6139, South Africa
[c] EaStCHEM School of Chemistry, University of Edinburgh, Joseph Black Building, David Brewster Road, Edinburgh EH93FJ, UK
[d] School of Laboratory Medicine and Medical Sciences, College of Health Sciences, University of KwaZulu-Natal, South Africa
[e] School of Chemistry, University of KwaZulu-Natal, Westville, 4401, South Africa
† These authors contributed equally.

relationship between non-covalent interactions and protein conformational stability.[14,15]

The PPI formed between Heat Shock Protein 90 (HSP90) and its co chaperone the HSP70-HSP90 organizing protein (Hop) facilitates the folding of numerous signalling intermediates and transcription factors, many of which are associated with invasive or aggressive tumours.[16] Furthermore, both proteins are important for maintaining proteostasis during the life-cycles of several viral families.[17–19]

Like many transient PPIs, the HSP90-Hop PPI is primarily mediated by a SLiM-domain interaction formed between the MEEVD pentapeptide motif found at the Hsp90 C-terminal domain ($Hsp90_{CTD}$) and the tetratrico peptide repeat-2A domain of Hop (Hop_{TPR2A}, Fig. 1A).[20,21] This interaction is dominated by a series of salt bridges formed between basic residues located within the binding groove of Hop_{TPR2A} and the acid rich MEEVD, including the so called 'carboxylate clamp' formed by the terminal aspartic acid residue (D5).

We have previously shown through an nMS investigation, that the association between acetylated Ac-MEEVD-OH (**1**, Fig. 1B) and

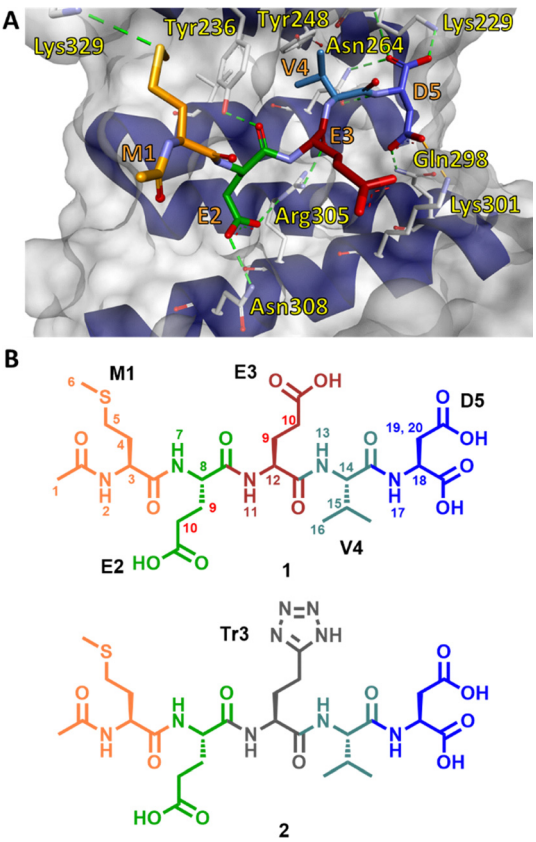

Fig. 1 (A) X-ray co-crystal structure of Ac-MEEVD-OH (**1**) bound to Hop_{TPR2A}. (PDB 1ELR). This interaction is dominated by a series of salt bridges formed between basic residues found in the binding groove of Hop_{TPR2A} and the acidic residues of **1** including the 'carboxylate clamp' formed by the terminal D5 residue. (B) Peptide **1** is an acetylated analogue of the naturally occurring MEEVD SLiM and has no PPI inhibitory activity. Peptide **2** is a PPI inhibitory non-natural analogue of **1**. Peptides are coloured per residue to match data shown in Fig. 8, 9 and 10. Numbering of structures correlates to numbering used for NMR structural elucidation.

Hop_{TPR2A} acts as a competent gas-phase proxy of the parent PPI.[22] We further demonstrated that a non-natural analogue of **1**, in which the E3 residue had been replaced with a tetrazole containing isostere (Tr3, **2**), bound to Hop_{TPR2A} with similar affinity to **1**, and that both peptides interact competitively.[22] In addition, we showed that despite the apparent similarly in binding affinity, peptide **2** disrupted the $Hsp90_{CTD}$–Hop_{TPR2A} interaction in a dose dependent fashion (pIC_{50} 6.5) while **1** was inactive. Through further investigation, we showed that peptide **2** was capable of inhibiting the full length HSP90-Hop PPI (63% at 100 μM).[22,23] Additional structure activity relationship (SAR) analysis focused on the $Hsp90_{CTD}$–Hop_{TPR2A} interaction (Fig. 2) showed that alteration of the amino acid sequence of peptide **2** (*e.g.* **3**), epimerization of the Tr3 (**4**), or replacement of D5 with a tetrazole isostere (**5**) was not generally well tolerated. However, moderate PPI inhibitory activity was retained in cases where Tr3 was replaced, with an aromatic amino acid (*e.g.* **6** [45% at 100 μM] and **7** [37% at 100 μM])[23] suggesting a degree of interactive plasticity in this region, and an important window for optimization in an otherwise narrow scope. It was further confirmed through immunoprecipitation assays that **2** interacted with Hop_{TPR2A} in cell lysates.[23]

While compound **2** seemingly suffered from poor cellular penetration, tethering **2** to a cell penetrating peptide translated into disruption of Kaposi sarcoma-associated herpesvirus (KSHV) lytic replication *in vitro*. This included reduced expression of KSHV lytic genes, diminished viral load and inhibition of the production of infectious virions at non-cytotoxic concentration.[23] Together these investigations, provided a compelling case that the HSP90-Hop PPI is an important potential host based target for developing KSHV therapeutics. However, despite its promise as a HSP90-Hop PPI modulator, the utility of peptide **2** as a *bona fide* inhibitor of KSHV lytic replication is constrained by the permeability challenges noted by us, in addition to likely pharmacokinetic liabilities, commonly associated with peptide therapeutics.[24] Overcoming these shortcomings

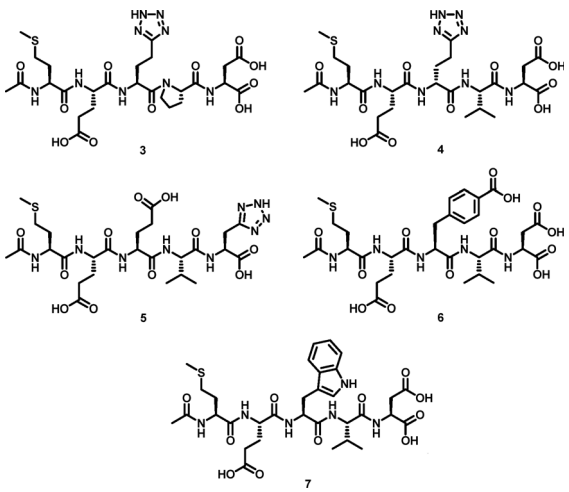

Fig. 2 Selected peptides from a previously reported SAR study which indicated that apart from some interaction plasticity at residue 3, (*e.g.* peptides **6** and **7**) very little alteration from the core motif is tolerated.[23]

would therefore require the application of an in-depth rational modification strategy. To that end, a key unanswered question that remained was why the E3 to Tr3 isosteric replacement resulted in contrasting PPI modulatory activity between peptides **1** and **2**, without imparting substantially different binding affinity?

We have previously postulated that the two peptides bind to Hop_{TPR2A} with varying poses, and it is the alteration of how specific residues interact with the target, and the possibility of conformational changes that underlies the biological activity of peptide **2**.[22,25] We reasoned therefore, that effective structural modification of **2** would be enhanced by improved insight into how regions of peptides **1** and **2** interact with Hop_{TPR2A}, and possibly, how the contrast of these interactions may be used as a fingerprint to guide future optimization campaigns. Accordingly, in this study, by combining nMS with two ligand-observed NMR techniques, namely Saturation Transfer Difference (STD) and Water Ligand Observed *via* Gradient Spectroscopy (WLOGSY) NMR, we were able to elucidate subtle variations in the interactions between peptides **1** and **2** with Hop_{TPR2A} thus providing a structural framework for future development of peptidomimetic HSP90-Hop PPI disruptors.

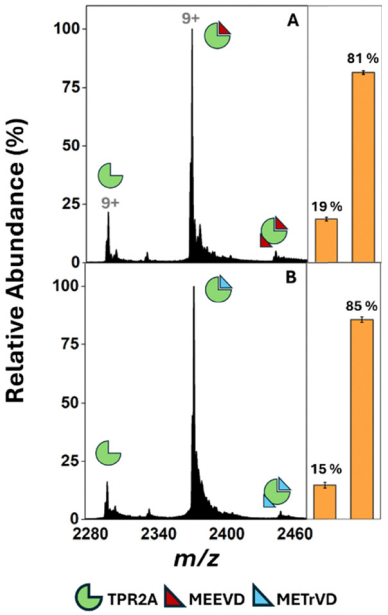

Fig. 3 nMS of the 9^+ charge state of a 1 : 5 mixture of Hop_{TPR2A} and peptides **1** (A), and **2** (B) in 50 mM NH_4OAc solution. Accompanying these spectra are complexation ratios calculated by combining the magnitude of bound and unbound protein across both the 8+ and 9+ charge state. These data are an average of three independent replicates. Error bars represent the standard deviation of these replicates. Despite neither peptide fully saturating Hop_{TPR2A} evidence of a second binding event emerged at this relative concentration.

Results and discussion

Native mass spectrometry

While the sensitivity of nMS is particularly useful for detecting weak non-covalent interactions, the magnitude of protein–ligand interaction can be significantly influenced by the concentration of NH_4OAc utilized during electrospray ionization.[26] Accordingly, as a preliminary optimization step, we conducted a dose-dependent nMS binding titration of peptides **1** and **2** at three different concentrations of NH_4OAc (50, 100, 200 mM). Here, Hop_{TPR2A} was retained at a constant final concentration of 10 μM and incubated with peptides at a ratio of 1 : 0.5, 1 : 1, 1 : 2 and 1 : 5 respectively. Mass spectra recorded with both peptides present in 5-fold excess (50 μM) showed that the bound species was over 80% abundant (Fig. 3A and B), and thus the Hop_{TPR2A} appeared not to be fully saturated. However, under our experimental conditions we observed the emergence of a peak corresponding to a second (likely non-specific) binding event and therefore used a ligand concentration of 50 μM as a titration end point. A double reciprocal plot was used to estimate the dissociation constants (K_d) of both peptides in each NH_4OAc solution (Fig. S1). With respect to peptide **1** binding, negligible variation in K_d was observed between the 50 mM (7.1 μM) and 100 mM (6.3 μM) NH_4OAc experiments. Furthermore, these data were largely in line with a previously reported K_d of peptide **1** binding to Hop_{TPR2A} (11 μM) determined *via* isothermal titration calorimetry.[27] However, ligand binding was negatively impacted when nMS experiments were conducted in 200 mM NH_4OAc, with the estimated K_d increasing to 23 μM.

Repeating these experiments using peptide **2**, confirmed our previous assertion that peptides **1** and **2** bind to Hop_{TPR2A} with similar efficiency, where in 50 and 100 mM NH_4OAc, K_d values were estimated at 7.1 and 5.8 μM respectively, while in 200 mM NH_4OAc, the K_d was again negatively impacted. Given the limited variation in the data collected from solutions in 50 and 100 mM NH_4OAc we opted to conduct all subsequent nMS experiments in 50 mM NH_4OAc.

It must be noted when using double reciprocal plots to estimate K_d, that data collected at low substrate concentrations has a disproportionate influence on the slope of the best fit line. This means that measurement errors are amplified in this region of the graph and limits the utility of this approach for the quantification of association kinetics.[28] However, given the comparability of our K_d values to literature values, the double reciprocal approach provided satisfactory evidence that our nMS methodology was suitable for obtaining reliable binding information.

Following this assessment, we utilized native IM-MS to investigate changes in arrival time distributions, and by extension molecular topology of Hop_{TPR2A} resulting from ligand binding (Fig. 4A). It is generally accepted that lower charge state ions provide the most accurate reflection of liquid phase conformation.[29] For this reason, we focussed our IM analysis on the 8+ charge states of our mass spectra.

The arrival time distribution of apo Hop_{TPR2A} revealed the presence of both a compact conformer (*C*) at a shorter drift time, and an extended conformer (*E*) at a longer drift time. By integrating the arrival time distribution curves, we determined that 34% of Hop_{TPR2A} remained as the *E* conformer (Table S1).

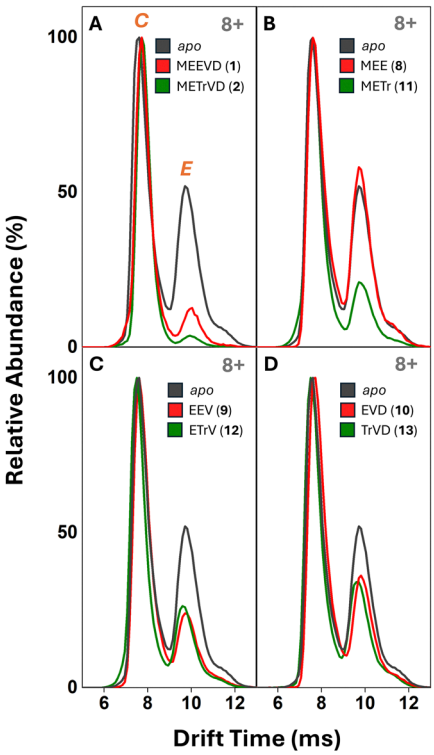

Fig. 4 (A) Arrival time distributions of the 8+ charge state of the native mass spectra of *apo* Hop_{TPR2A} and the complexes with peptides **1** and **2** showing the presence of a compact (*C*) and extended (*E*) conformer of Hop_{TPR2A}. These data indicate that complexation with peptides **1** and **2** promotes the gas-phase stability of the *C* conformer. (B)–(D). Arrival time distributions of the 8+ charge state of the native mass spectra of peptide '3-mers' **8–13** in complex with Hop_{TPR2A} overlaid with the data for *apo* Hop_{TPR2A}. Most notably, peptide **8** (MEE) was unable to influence gas phase stability of the *C* conformer.

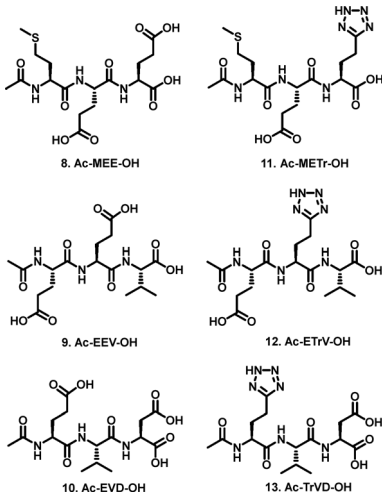

Fig. 5 "3-mer' peptides **8–13** derived from parent peptides **1** and **2**.

These data indicated either that Hop_{TPR2A} possesses a measure of conformational flexibility or that under our electrospray conditions Hop_{TPR2A} undergoes some degree of unfolding during transmission into the gas phase.

By contrast, incubation with peptides **1** (12%) and **2** (5%) saw a significant reduction in the relative abundance of the *E* conformer. The generally accepted dogma is that TPR domains are rigid scaffolds that do not undergo significant conformational changes upon ligand binding.[30] However, contemporary opinion suggests that in certain instances peptide binding can induce dramatic conformational changes to the arrangement of TPR domains.[31] While it is not clear from these data whether Hop_{TPR2A} is more conformationally flexible than previously thought, or whether SLiM binding induces significant conformational change, these data do strongly indicate that SLiM binding imparts significant gas-phase stability to the compact conformation of Hop_{TPR2A} and that this effect is particularly pronounced for peptide **2**.

With a view to elucidating regio-dependent contributions to target binding, we synthesized two cohort of overlapping '3-mers' (**8–13**, Fig. 5) derived from parent peptides **1** or **2** and all featured either the E3 or Tr3 residue. Their interaction with Hop_{TPR2A}, was assessed by nMS however, given the limitations of double reciprocal plots for estimating K_d values, binding affinity was assessed by percent binding for experiments conducted at a 1 : 5 molar ratio (Fig. 6 and 7). When incubated with 50 μM of peptide **13**, we again saw evidence of a second bound peptide, possibly due to non-specific binding.

Amongst this cohort, the best binding was observed for peptides **10** (17%) and **13** (18%). The most striking result however was the seemingly disproportionate reduction in target binding, where in all instances 3-mer binding was substantially reduced in comparison to their parent peptide despite retaining 60% of their sequence. Interpretation of the percent binding of 3-mers, **8** (5%), **9** (6%) and **10** (17%) in the context of peptide **1** indicated that the most significant contribution to Hop_{TPR2A} binding can likely be attributed to the presence of the terminal Asp residue, rather than a shortened peptide epitope. However, even with the contribution of the 'carboxylate clamp' the magnitude of binding of peptide **10** is still significantly impeded by sequence truncation and cannot be considered an efficient binding hot spot. This same trend was observed for 3-mers **11** (8%), **12** (6%) and **13** (18%).

Together these data suggest that rather being mediated by a dominant hot-spot interaction, efficient recognition of either peptides **1** or **2** by Hop_{TPR2A} is mediated by complimentary contributions along the full peptide sequence. Comparison of peptides across cohorts *e.g.* **8** (5%) *vs.* **11** (8%), **9** (6%) *vs.* **12** (6%) and **10** (17%) *vs.* **13** (18%) showed that even when reduced to smaller peptides, the E to Tr isosteric replacement did not make a significant impact on peptide binding, supporting the notion that the differences in biological activity observed between peptides **1** or **2** are not linked to differences in binding affinity.

Once more we utilized native IM-MS to interrogate the arrival time distributions of Hop_{TPR2A}–**3**-mer complexes. With the exception of peptide **8**, 3-mer binding resulted in a reduction in the relative abundance of the *E* conformer, compared to apo Hop_{TPR2A}, indicating some manner of binding induced stabilization (Fig. 4B–D, Table S1). However, the

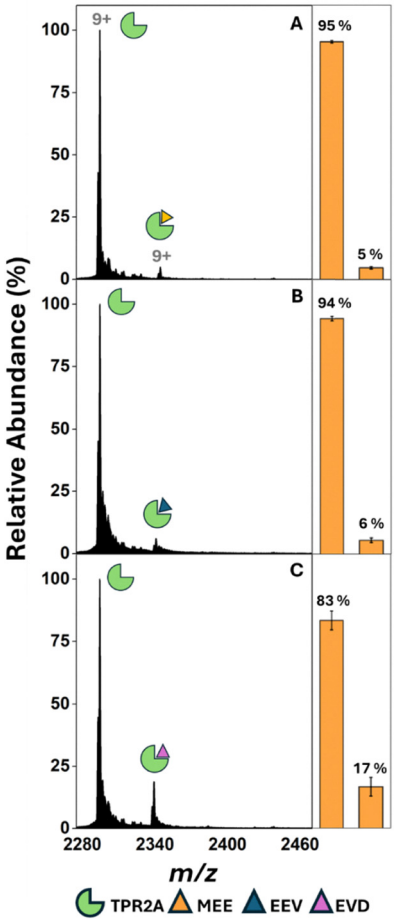

Fig. 6 nMS of the 9^+ charge state of a 1 : 5 mixture of Hop_{TPR2A} and peptides **8** (A), **9** (B) and **10** (C) in 50 mM NH_4OAc solution. Accompanying these spectra are complexation ratios calculated by combining the magnitude of bound and unbound protein across both the 8+ and 9+ charge state. These data are an average of three independent replicates. Error bars represent the standard deviation of these replicates. These data suggest that the loss of two amino acids from the parent sequence has a disproportionately negative impact on binding.

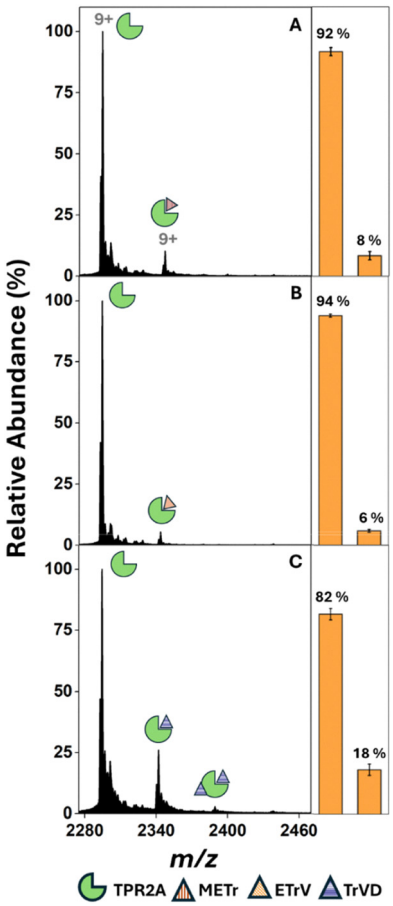

Fig. 7 nMS of the 9^+ charge state of a 1 : 5 mixture of Hop_{TPR2A} and peptides **11** (A), **12** (B) and **13** (C) in 50 mM NH_4OAc solution. Accompanying these spectra are complexation ratios calculated by combining the magnitude of bound and unbound protein across both the 8+ and 9+ charge state. These data are an average of three independent replicates. Error bars represent the standard deviation of these replicates The same negative influence on binding is observed as in Fig. 6.

stabilization effect, was not uniform and did not correlate to the Hop_{TPR2A} binding affinity shown in Fig. 3 and 4. This was exemplified by peptides **10** and **13**, which despite their superior binding affinity had a negligible impact on conformational stability (*E* conformer 34% and 25% respectively). Furthermore, in contrast to the binding data, comparison of the impact of the related pairs of peptides showed that the E to Tr isosteric replacement had a noticeable impact on arrival time distribution of the Hop_{TPR2A}–**3**-mer complexes (Table S1). This was particularly stark for the methionine containing peptides **8** and **11**. In the presence of peptide **8** (34%) the abundance of the *E* conformer was analogous to that observed for apo Hop_{TPR2A} while introduction of the tetrazole moiety in peptide **11** resulted in a noticeable reduction in the *E* conformer (15%). This suggests that the METr region of peptide **2**, enhances the conformational stabilising effect of SLiM binding, and that this effect, which may underpin the observed biological activity is not inherently linked to binding affinity.

Ligand-observed NMR

STD and WLOGSY NMR, both exploit the nuclear Overhauser effect (NOE) which together, provide information pertaining to the interacting epitope of a binding ligand, and water accessibility following binding.[32–34] In the context of transient PPIs, if each of the ^1H nuclei have been fully elucidated, these data effectively provide a fingerprint of SLiM-domain interactions, where subtle alterations in magnetization transfer, resulting from changes to either the target or interacting ligand can be detected at sub-residue resolution. For the purposes of assigning ^1H resonances, we numbered each relevant proton according to Fig. 1B. Beginning with a spectral analysis of the Hop_{TPR2A}–**1** complex (Fig. S10 and Table S2), TOCSY NMR was used to assign correlating protons within an amino acid residue, while NOESY NMR allowed for amido NH resonances to be assigned *via* through space correlation to the α-proton of the neighbouring amino acid. Our assignment origin was the V4 residue, where the isopropyl methyl signals (H-16, δ 0.78) were clearly distinguishable. This then allowed us to assign the

V4 amido NH (H-13, δ8.05) and α-protons (H-14, δ4.11), respectively.

NOESY correlations between H-14 and the D5 amido NH (H-17, δ7.87), and H-13 and the E3 α-proton (H-12, δ4.30) allowed assignment of both residues, which in turn, facilitated the TOCSY-assisted assignment of the D5 α-protons (H-18, δ4.24), the diastereotopic D5 methylene protons H-19 and H-20 (δ2.45, 2.55) and the E3 amido NH (H-11, δ8.31). Through this approach, we were further, able to assign the E2 α-proton (H-8, δ4.21), alongside the outstanding M1 residues, including the M1 NH (H-2, δ8.21), α- (H-3, δ4.33), *S*-methyl (H-6, δ1.90) and terminal acetyl (H-1, δ1.98). However, the corresponding β (H-9) and γ (H-10) positions on the E2 and E3 side chains were indistinguishable and were assigned the same residue number (Table S2 and Fig. 1B).

We subsequently applied this template to peptide **2**, where again, we successfully distinguished proton resonances apart from the corresponding β and γ positions on the E2 and Tr3 side chains, which were also assigned the same number. We proceeded to fingerprint peptide binding through STD and WLOGSY NMR. In recording STD NMR data, two separate experiments are acquired. The first, (on-resonance) spectrum, applies selective radio frequencies to the protein where magnetization is transferred from the protein to the bound ligand *via* NOE and the second (off-resonance) spectrum is acquired without the selective irradiation of the protein. Subtracting the signal intensity of the off-resonance spectrum signals, from that observed in-resonance spectrum results in the STD spectrum, where only signals magnetized *via* the NOE effect remain (Fig. 8). Relative quantification of STD efficiency, (determined as a percentage of the largest STD signal) is indicative of relative proximity to the protein surface and (Fig. 9).

Analysis of the STD NMR of the Hop_{TPR2A}–**1** complex showed that all identifiable proton resonances were in sufficient proximity to the protein to undergo magnetization *via* NOE.

This suggested that all these regions contributed in some fashion to the binding of peptide **1**, thus supporting the nMS binding data. The mean STD intensity was calculated as 23% per resonance, and this value was used as a lower limit, for characterizing significant binding contributions (Fig. 9 and Table S2). STD intensity was the most pronounced for the E2 α-proton (H-8, 100%) indicating particularly close contact to the protein surface. Signal intensities of the α-protons of V4 (H-14, 35%), M1 (H-3, 25%), E3 α-proton (H-12, 23%) and the D5 NH (H-17, 26%) all equalled or exceeded the mean intensity (23%) and were considered comparatively important interacting regions.

Similarly, all identifiable proton resonances in the Hop_{TPR2A}–**2** complex showed STD NMR signals, also with a mean intensity of 23%. The E2 α-proton signal was again found to have a relative intensity of 100%, while the V4 (43%) and M1 (37%) α-protons were also identified as prominent interacting regions. While in comparison to the Hop_{TPR2A}–**1** complex, the relative intensity of the D5 NH, was substantially reduced (10%), the D5 α-proton signal (H-18, 37%), emerged as a significant relative contributor, indicating, a slight alteration in binding conformation at the D5 residue. The most significant change in the STD spectral data between the complexes of **1** and **2** with Hop_{TPR2A} was observed for the Tr3 α-proton (H-12, 100%) whose relative signal intensity was equal to H-8 (Fig. 9). This shift indicated a substantial alteration in protein proximity, resulting from the tetrazole isosteric replacement.

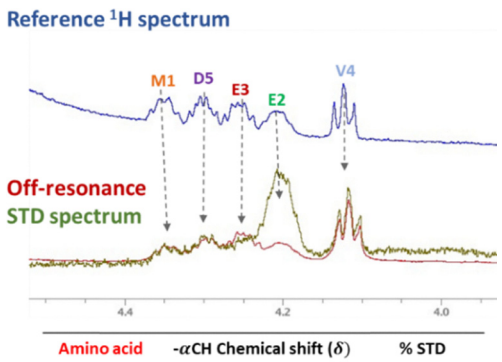

Amino acid	-αCH Chemical shift (δ)	% STD
M1	4.33 ppm	25
E2	4.21 ppm	100
E3	4.24 ppm	23
V4	4.12 ppm	35
D5	4.30 ppm	16

Fig. 8 Stacked 1D ^{1}H expansions of Hop_{TPR2A}–**1** complex. The reference ^{1}H spectrum is shown in blue, while the off-resonance and STD spectra are shown in red and green, respectively. The STD amplification factor for each unique signal was calculated as the percentage of signal in the off-resonance spectra over the signal intensity in the STD spectrum.

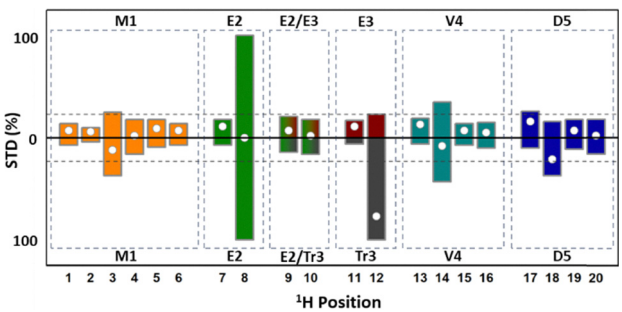

Fig. 9 Comparative analysis of STD NMR data of the Hop_{TPR2A}–**1** (phased up) and Hop_{TPR2A}–**2** (phased down) complexes, respectively. Each residue is boxed off and shown in a distinct colour for clarity. The ambiguously assigned H-9 and H-10 protons are grouped together. ^{1}H position correlates to numbering in Fig. 1B. The horizontal dashed line depicts the mean STD intensity for each experiment. The height of each bar corresponds to the relative magnitude of the STD signal, whereas the white circles indicate the difference in magnitude for corresponding signals between the Hop_{TPR2A}–**1** and Hop_{TPR2A}–**2** experiments. In both complexes, the E2 α-proton (H-8) was the most prominent signal, indicating a central role in binding for both peptides. The most noticeable change was observed between the H-12 protons of each peptide, suggesting that the Tr3 α-proton makes a significant new interaction with Hop_{TPR2A}. In addition, the changes observed between H-17 and H-18 for peptides **1** and **2**, suggest a change in conformation in this region.

Despite these alterations, the STD intensities of unassigned E2/E3 and E2/Tr3 residues H-9 and H-10 were both lower than their respective means and were considered to make comparatively negligible contributions to binding.

We then conducted a WLOGSY analysis of both complexes. During WLOGSY acquisitions, polarization is transferred from water molecules to bound ligands by NOE. An NOE transfer from protein-bound water will lead to signal suppression or inversion (−ve WLOGSY), while signals from nuclei that interact with bulk water will not be inverted (+ve WLOGSY).[35] Quantification of this effect provides insight into the relative strength of interaction of specific regions of a bound-ligand *via* its interaction with protein-bound waters. With respect to the Hop_{TPR2A}–**1** complex, and in line with STD NMR data, all peptide signals were either suppressed or inverted (Fig. S11). The most pronounced WLOGSY inversions were observed for the amido NH's of M1 (−87%) and E2 (−100%) followed by a slight reduction in intensity for the E3 NH (−76%), and a less substantial reduction for the V4 NH (−14%) (Fig. 10). While the signal was suppressed, no inversion was observed for the D5 NH. In addition, a substantial WLOGSY inversion was observed for the M1 methyl (H-6, −52%), while a moderate inversion was observed for the valine methyl signals (H-16, −26%). One additional weak WLOGSY inversion was observed for the *N*-acetamide (H-1, −14%).

With respect to the Hop_{TPR2A}–**2** complex, the patterns of the WLOGSY inversions generally mirrored that of Hop_{TPR2A}–**1**. However, the relative magnitude of the signals on at the M1 α position (-95%) Tr3 NH (−95%) was generally enhanced.

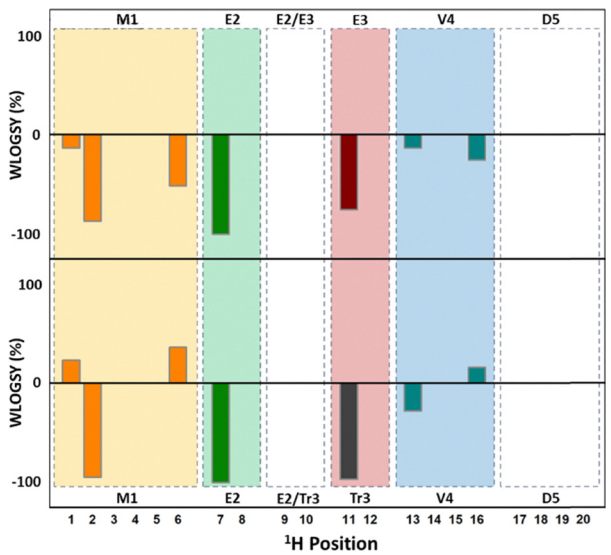

Fig. 10 Comparative analysis of WLOGSY NMR data of the Hop_{TPR2A}–**1** (top) and Hop_{TPR2A}–**2** (bottom) complexes respectively. Figure formatting matches Fig. 9. Regions where WLOGSY signals were detected are highlighted in colour. In both complexes, the E2 NH proton (H-7) was the most prominent signal, again like the STD data indicating a central role for E2 in binding for both peptides. The changes in WLOGSY signals, particularly the presence of +ve signals for H-1, H-6 and H-16, indicate substantial changes in the interaction of M1 and V4 with binding site waters for peptide **2** when compared to peptide **1**.

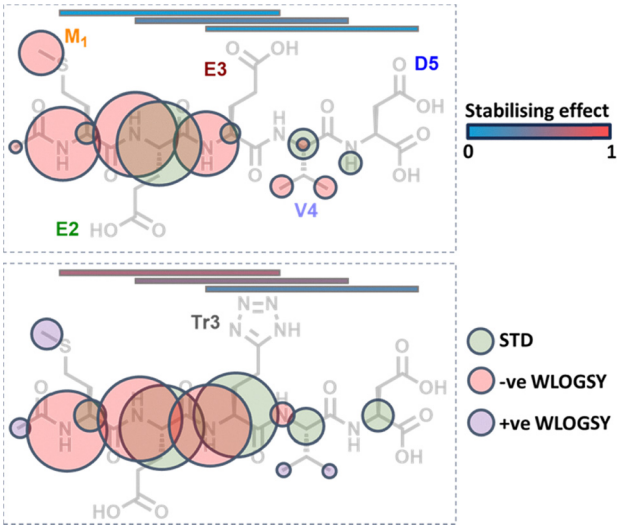

Fig. 11 Summary of the SLiM observed 'fingerprinting' of the Hop_{TPR2A}–**1** (top) and Hop_{TPR2A}–**2** (bottom) complexes, respectively. The coloured bars represent the stabilising effect of each overlapping 3-mer, relative to the data obtained for apo Hop_{TPR2A} (0) and the Hop_{TPR2A}–**2** complex (1). Calculations in Table S1. Bubble colour represents the mechanism of NOE magnetization, while bubble diameter is proportional to signal intensity. STD signals below the experimental mean and WLOGSY signals, which were supressed to 0% but not inverted were excluded.

(Fig. 10). Interestingly, the H-1, H-6 (M1), and H-14 (V4) nuclei in the Hop_{TPR2A}–**2** complex appeared as +ve WLOGSY signals, suggesting that these nuclei were experiencing reduced NOE transfer from bound waters. This contrasts to the corresponding signals emanating from the Hop_{TPR2A}–**1** complex indicating a variation in water coordination in this region at the binding site. Owing to the substantially weaker binding observed for peptides **3–8**, and the extremely high concentrations required to saturate the protein we did not feel that repeating these experiments using peptides **3–8** was feasible.

Based on the outcomes of the IM hyphenated nMS and ligand observed NMR experiments, we plotted a summative ligand-observed binding 'fingerprint' (Fig. 11). This figure illustrates that despite providing no significant enhancement to binding affinity, the E3 to Tr3 isosteric replacement results in variations in the proximity of different regions of peptides **1** and **2** to the surface of Hop_{TPR2A} and their interaction with binding site water molecules. This phenomenon was especially pronounced in the regions surrounding the M1 and Tr3 amino and is indicative of a relative shift to the binding orientation of this region of peptide **2**. Importantly, this data supports the nMS study in which peptide **11**, which contains both the M1 and Tr3 residues, was found to provide the biggest contribution to maintaining Hop_{TPR2A} in a compact conformation.

Conclusions

As part of our ongoing investigation of the HSP90-Hop PPI as a host-based target for anti-viral drug discovery, this study sought to unravel, how, despite similar binding affinity for Hop_{TPR2A}, peptides **1** and **2** which differ only by an isosteric replacement

of the carboxylic acid moiety of E-3 to a tetrazole, display contrasting PPI modulatory capacities. Through the synthesis of a series of 3-mers, representative of the parent peptides and incorporating a blend of native IM-MS, and ligand-observed NMR experiments we were able to elucidate subtle variations in how specific regions of peptides **1** and **2**, interacted with Hop_{TPR2A} and their influence on target conformational stability. Cumulative data acquired in previous studies have alluded to the possibility that the variation in PPI modulatory activity is an artifact of altered binding mode and its influence on target conformation.[22,25] The results of this study provide finer grained support of that notion and a structural fingerprint against which future development of HSP90-Hop PPI disruptors can be based. Given the disproportionate fall off in binding affinity observed amongst the 3-mers, it is likely that for ligands to possess sufficient target occupancy for PPI modulation to occur, they would likely need to span the full binding groove of Hop_{TPR2A}. Therefore, rather than focusing on drug-like small molecules, future optimization may find more success through peptidomimetics which can anchor in the binding site, and mimic the key interactions made by M1 and Tr3. One potential strategy includes incorporating cross-links to lock the peptide in a biologically active conformation.[36] Alternatively, alteration of the amide backbone, such as that observed with small 5-membered heterocycles offers the opportunity to present amino acid side chains in a preferred relative conformation.[37] These are just a two of many strategies employed for the rational development of peptidomimetics from SLiMs. Finally, this study showed that binding affinity in isolation is not necessarily a reliable predictor of PPI modulatory capacity. We have thus provided a general, resource efficient workflow for elucidating subtle interfacial characteristics of SLiM-domain interactions, which can be exploited to rationally modulate transient PPIs in the contemporary drug discovery landscape.

Author contributions

Peptide synthesis, purification and characterization was led by TKR, and assisted by JCS, BGdlT and FA. NMS studies were led by TKR and assisted by SKM and DJC. NMR studies were led by DAK and assisted by MR. Protein expression and purification was conducted by RM and ALE. Paper drafting was conducted by TKR and CGLV. All authors contribute to review and editing. Project conceptualization and coordination was conducted by CGLV.

Conflicts of interest

There are no conflicts to declare.

Data availability

All relevant data used in the study are available in the article or in the supplementary information (SI) provided alongside it. Any additional data is available on request from the corresponding authors. Supplementary information is available. See DOI: https://doi.org/10.1039/d6cb00112b.

Acknowledgements

The authors acknowledge research funding from the National Research Foundation (NRF, Grant No. CPRR240314209156), The Poliomyelitis Research Fund (PRF, Grant No. 25/87), a Scottish Funding Council (SFC) International Science Partnership Fund, the University of Cape Town (UCT), Rhodes University, the South African Research Chairs Initiative of the Department of Science, Technology and Innovation (DSTI/NRF, Grant No. 98566) a South African Medical Research Council (SA-MRC) Self-Initiated Research Grant, an MRC Africa Research Leaders award (MR/V030701/1) which is jointly funded by the UK Medical Research Council (MRC) and the UK Foreign, Commonwealth & Development Office (FCDO) under the MRC/FCDO Concordat agreement and is carried out in the frame of the Global Health EDCTP3 Joint Undertaking and Future Leaders – African Independent Research (FLAIR), a partnership between the African Academy of Sciences and the Royal Society that is funded by the UK Government as part of the Global Challenge Research Fund (GCRF). T. D. and S. M. gratefully acknowledge funding in the form of an NRF Freestanding Bursary and a UCT Science Faculty Scholarship respectively.

References

1 H. C. Jubb, A. P. Pandurangan, M. A. Turner, B. Ochoa-Montaño, T. L. Blundell and D. B. Ascher, *Prog. Biophys. Mol. Biol.*, 2017, **128**, 3–13.
2 F. Cheng, J. Zhao, Y. Wang, W. Lu, Z. Liu, Y. Zhou, W. R. Martin, R. Wang, J. Huang, T. Hao, H. Yue, J. Ma, Y. Hou, J. A. Castrillon, J. Fang, J. D. Lathia, R. A. Keri, F. C. Lightstone, E. M. Antman, R. Rabadan, D. E. Hill, C. Eng, M. Vidal and J. Loscalzo, *Nat. Genet.*, 2021, **53**, 342–353.
3 M. Zhong, G. M. Lee, E. Sijbesma, C. Ottmann and M. R. Arkin, *Curr. Opin. Chem. Biol.*, 2019, **50**, 55–65.
4 H. Nada, Y. Choi, S. Kim, K. S. Jeong, N. A. Meanwell and K. Lee, *Signal Transduct. Target. Ther.*, 2024, **9**, 341.
5 C. G. L. Veale and D. J. Clarke, *Trends Chem.*, 2024, **6**, 377–391.
6 A. Ballone, R. A. Lau, F. P. A. Zweipfenning and C. Ottmann, *Acta Crystallogr., Sect. F: Struct. Biol. Commun.*, 2020, **76**, 501–507.
7 F. Centorrino, A. Ballone, M. Wolter and C. Ottmann, *FEBS Lett.*, 2018, **592**, 1211–1220.
8 S. P. Van Wier and A. M. Beekman, *Chem. Soc. Rev.*, 2025, **54**, 1684–1698.
9 Y. Li, C. H. Trinh, A. Acevedo-Jake, D. Gimenez, S. L. Warriner and A. J. Wilson, *Biochem. J.*, 2024, **481**, 945–955.

10 J. Bellamy-Carter, M. Mohata, M. Falcicchio, J. Basran, Y. Higuchi, R. G. Doveston and A. C. Leney, *Chem. Sci.*, 2021, **12**, 10724–10731.
11 D. Brancaccio, S. Di Maro, L. Cerofolini, S. Giuntini, M. Fragai, C. Luchinat, S. Tomassi, A. Limatola, P. Russomanno, F. Merlino, E. Novellino and A. Carotenuto, *ACS Med. Chem. Lett.*, 2020, **11**, 1047–1053.
12 C. J. A. Verhoef, D. F. Kay, L. van Dijck, R. G. Doveston, L. Brunsveld, A. C. Leney and P. J. Cossar, *Chem. Sci.*, 2023, **14**, 6756–6762.
13 E. Barile and M. Pellecchia, *Chem. Rev.*, 2014, **114**(9), 4749–4763.
14 J. Stojko, S. Fieulaine, S. Petiot-Bécard, A. Van Dorsselaer, T. Meinnel, C. Giglione and S. Cianférani, *Analyst*, 2015, **140**, 7234–7245.
15 C. E. Eyers, M. Vonderach, S. Ferries, K. Jeacock and P. A. Eyers, *Curr. Opin. Chem. Biol.*, 2018, **42**, 167–176.
16 A. L. Edkins, *Top. Med. Chem.*, 2016, **19**, 21–54.
17 J. Hu, D. Flores, D. Toft, X. Wang and D. Nguyen, *J. Virol.*, 2004, **78**, 13122–13131.
18 E. Kirigin, M. O. Okpara, L. Matandirotya, J.-L. Ruck, F. Weaver, Z. Jackson, A. Chakraborty, C. G. L. Veale, A. Whitehouse and A. L. Edkins, *J. Gen. Virol.*, 2024, **105**, 002053.
19 B.-P. Mohl and P. Roy, *J. Virol.*, 2019, **93**, e00898-19.
20 A. Brinker, C. Scheufler, F. Von Der Mülbe, B. Fleckenstein, C. Herrmann, G. Jung, I. Moarefi and F. Ulrich Hartl, *J. Biol. Chem.*, 2002, **277**, 19265–19275.
21 C. Scheufler, A. Brinker, G. Bourenkov, S. Pegoraro, L. Moroder, H. Bartunik, F. U. U. Hartl and I. Moarefi, *Cell*, 2000, **101**, 199–210.
22 C. G. L. Veale, M. Mateos-Jiménez, M. C. Vaaltyn, R. Müller, M. P. Makhubu, M. Alhassan, B. G. de la Torre, F. Albericio, C. L. Mackay, A. L. Edkins and D. J. Clarke, *Chem. Commun.*, 2021, **57**, 10919–10922.
23 M. O. Okpara, M. C. Vaaltyn, J. L. Watson, M. Alhassan, F. Albericio, B. G. de la Torre, D. J. Clarke, C. G. L. Veale and A. L. Edkins, *ACS Infect. Dis.*, 2024, **10**, 3853–3867.
24 L. Lombardi, V. Del Genio, F. Albericio and D. R. Williams, *Chem. Rev.*, 2025, **125**, 7099–7166.
25 C. G. L. Veale, A. Chakraborty, R. Mhlanga, F. Albericio, B. G. de la Torre, A. L. Edkins and D. J. Clarke, *Chem. Commun.*, 2024, **60**, 5844–5847.
26 A. F. M. Gavriilidou, B. Gülbakan and R. Zenobi, *Anal. Chem.*, 2015, **87**, 10378–10384.
27 C. Scheufler, A. Brinker, G. Bourenkov, S. Pegoraro, L. Moroder, H. Bartunik, F. U. Hartl and I. Moarefi, *Cell*, 2000, **101**, 199–210.
28 R. B. Martin, *J. Chem. Educ.*, 1997, **74**, 1238–1240.
29 J. T. S. Hopper, K. Sokratous and N. J. Oldham, *Anal. Biochem.*, 2012, **421**, 788–790.
30 V. Parashar, P. D. Jeffrey and M. B. Neiditch, *PLoS Biol.*, 2013, **11**, e1001512.
31 A. Perez-Riba and L. S. Itzhaki, *Curr. Opin. Struct. Biol.*, 2019, **54**, 43–49.
32 S. Monaco, J. Angulo and M. Wallace, *J. Am. Chem. Soc.*, 2023, **145**, 16391–16397.
33 R. Nepravishta, S. Walpole, L. Tailford, N. Juge and J. Angulo, *ChemBioChem*, 2019, **20**, 340–344.
34 S. Monaco, L. E. Tailford, N. Juge and J. Angulo, *Angew. Chem., Int. Ed.*, 2017, **56**, 15289–15293.
35 C. J. R. Bataille, T. H. Rabbitts and T. D. W. Claridge, *Bio-protocol*, 2020, **10**, e3666.
36 A. Glas, D. Bier, G. Hahne, C. Rademacher, C. Ottmann and T. N. Grossmann, *Angew. Chem., Int. Ed.*, 2014, **53**, 2489–2493.
37 E. Ko, J. Liu, L. M. Perez, G. Lu, A. Schaefer and K. Burgess, *J. Am. Chem. Soc.*, 2011, **133**, 462–477.